Defence Research and Development Canada | Recherche et développement pour la défense Canada

DRDC | RDDC
technologysciencetechnologie

DRDC External Publication

Produced for: 34th International Symposium on Military Operational Research (ISMOR)
Royal Holloway, University of London
London, UK
18 – 21 July 2017

Determination of Naval Gun System Firing Patterns to Combat Manoeuvring Surface Targets

Peter J. Young[1]
Centre for Operational Research and Analysis
Defence Research and Development Canada

Abstract

Small attack boats pose a significant threat to naval ships due to their fast approach speeds, manoeuvrability and ability to deploy in numbers that may overwhelm ship defences. Naval gun systems, such as the 57 mm gun on the Halifax class frigates, can engage such targets by firing salvos of fragmenting rounds. Salvo kill probabilities may be maximised through employment of firing patterns designed to disperse rounds over the projected movement zone of a manoeuvring target. This paper summarises computational methods developed to determine salvo kill probabilities against manoeuvring surface targets. Discrete probability distributions are constructed for the warhead lethal zone and the projected target movement zone, these taking into account dispersion errors for warhead ballistics and target tracking errors. Numerical methods are then employed to determine aim point offsets for individual rounds of a salvo so that salvo kill probability can be maximised. Results are presented illustrating the range dependence of optimised firing patterns against manoeuvring surface targets. The work is supporting development of gun system firing patterns for the Royal Canadian Navy through further Monte Carlo simulation of warhead fly-out/detonation, live firing field trials and multi-threat engagement analysis.

Acknowledgements: To Mr. RWH McKillip, CFMWC, who contributed to problem formulation and provided domain expertise, and to the ISMOR referees for their constructive feedback and advice.

[1] Operational Research Team, Canadian Forces Maritime Warfare Centre (CFMWC), CFB Halifax, Nova Scotia, Canada. Email: peter.young2@forces.gc.ca

Introduction

A significant asymmetric threat to Maritime operations in littoral waters is that posed by small attack boats, generally termed Fast Inshore Attack Craft (FIAC). These boats can be employed in numbers and are difficult to engage due to their high approach speeds and manoeuvrability. Naval gun systems, such as the 57 mm gun on the Halifax class frigates, are a primary means of defence against such threats. Given possible swarm attacks, naval gun systems can engage these threats by firing salvos of fragmenting rounds. Engagement success can be improved through employment of firing patterns designed to counter possible target manoeuvres.

This paper provides an overview of techniques developed to determine salvo firing patterns that maximise kill probability against manoeuvring surface targets. The work builds on concepts given in [1] for computing firing patterns against manoeuvring surface targets given uncertainties in target track, target manoeuvre and dispersion errors affecting the projectile's trajectory. Results using illustrative data are provided to demonstrate the methodology and give an indication of some of the characteristics of firing patterns.

Problem Overview

Problem scope is restricted to firing of a fragmenting warhead with time mode fusing against a single surface target. Warhead detonation time is set by the gun system at the time of firing so that an airburst relative to the aim point is achieved. The first work objective is to determine the probability of killing a manoeuvring surface target through firing a salvo of rounds in a single, time sequenced burst. Individual rounds in the salvo may be given unique offsets from an aim point derived using the target track. A second work objective is to determine optimal aim point offsets for each round in the salvo so as to maximise the salvo probability of kill. The number of rounds in a salvo and the aim point offsets for the rounds constitute a firing pattern.

Problem Description

A naval gun system is engaging a target based on available target track information. The target track is obtained from ship sensors and comprises estimates of the target state (location and velocity vector) at the time of firing. The track therefore incorporates uncertainties arising from the sensor measurement process.

At the time of firing the naval gun system will compute aiming parameters, in particular azimuth and quadrant elevation angles of the barrel and detonation time for a time fused warhead, so that the projectile trajectory will intercept the projected location of the target. For an air burst fragmenting warhead, the projectile's trajectory may be adjusted for a specified offset in height above the surface and lead distance ahead of the target so that the warhead`s effect against the target is maximised.

Once fired, the projectile will fly out along a trajectory dependent on projectile ballistic properties (muzzle velocity, mass, aerodynamic coefficients), atmospheric conditions (air temperature, density and pressure) and actual aiming angles. The resultant trajectory in combination with the warhead fusing mechanism will define a detonation point. Given dispersion errors in aiming and other parameters, e.g. muzzle velocity, the detonation point will have some error offset from the aim point.

Upon detonation, the fragmenting warhead will disperse fragments in a characteristic fan pattern with 360^0 rotational symmetry about the primary axis of the warhead. A number of these

fragments may impact the target, this being dependent on the actual detonation point, the actual target location at the time of detonation, and the target size. Some of the impacting fragments may have sufficient energy to cause damage or kill the target, this being dependent on fragment impact velocity, mass and the vulnerability of the target.

Successful engagement of a target becomes more challenging at larger ranges as tracking errors lead to a greater uncertainty in target location and firing dispersion errors lead to a greater variance in actual detonation points about a desired aim point. This is further complicated by possible target manoeuvres taken after the time of firing but before the detonation time.

Target tracking errors at the time of firing define an area of possible target location. A target movement zone is constructed by projecting possible target locations forward in time for the flight time of the projectile and taking into account possible target manoeuvres during this time. The target movement zone represents possible target locations at the time of warhead detonation. As the warhead has a limited lethal zone, it will only affect the target for a subset of possible locations in the movement zone. To compensate for this, a number of rounds may be fired in a pattern spread across the movement zone. The aim of this work is to analyse such firing patterns in order to determine those that maximise the probability of killing the target.

Analysis Approach

The problem is stochastic in nature and is approached using tools from statistical theory [2]:

- The uncertainties in target track can be represented as random variables. These variables are used to define joint probability distributions for the target track at the time of firing and the target movement zone at the time of warhead detonation. The target movement zone takes into account further random variables adopted to account for possible target manoeuvres.
- The dispersion errors present in the gun at the time of firing are also represented as random variables. The ballistics equations for projectile fly-out reflects a function of the input random variables for the dispersion errors and yields output random variables for warhead location and velocity vector at the time of detonation. A joint probability distribution for the output random variables is obtained through a transformation of the input joint probability distribution using the ballistic equations.
- A probabilistic model is used to construct the lethal zone for a detonating warhead. This warhead lethal zone is aggregated across the joint probability distribution for detonation points about the aim point to yield an aim point lethal zone.
- The aim point lethal zone is integrated across the target movement zone to yield the probability of kill for a single round and a given aim point.
- The target movement zone is updated to reflect target survivability after detonation of the first round. It is then stepped forward in time to the time point of the second round detonation. The lethal zone for this round with its aim point is generated and then integrated across the updated target movement zone to yield the probability of kill for the second round. This step is then repeated for each subsequent round in the salvo.
- The overall salvo probability of kill is obtained by summing the probabilities of kill for the individual rounds in the salvo.

Computational techniques have been developed to implement the above approach. Joint probability distributions for the target movement zone and the aim point lethal zone are constructed numerically and used to calculate salvo probability of kill. Numerical and analytical methods are then explored to investigate how salvo firing patterns can be optimised so as to

yield a maximum probability of kill. The following sections provide details and illustrative results for this. Concepts and implementations from statistical theory are introduced and discussed as needed through these sections.

Target Representation

The target is considered to have point location, constant 1 m^2 size from all aspects (for vulnerability assessment) and constant velocity.

Target Tracking

The ship`s Fire Control System (FCS) will obtain estimates of the range to the target, target bearing angle relative to the ship`s heading, target velocity, and target heading. These estimates are assumed to be normally distributed about the actual values. They may be represented as samples with associated probabilities from the following independent normal random variables[2] with discrete approximations[3]:

- Range to target: $R_T \sim \mathrm{N}\left(\mu_{R_T}, {\sigma_{R_T}}^2\right)$; $\overline{R_T} = \left\{r_{T\_i}, P_{R_{T\_i}}\right\}, i = 1 \dots N_{R_T}$.
- Bearing to target: $\Theta_T \sim \mathrm{N}\left(\mu_{\Theta_T}, {\sigma_{\Theta_T}}^2\right)$; $\overline{\Theta_T} = \left\{\theta_{T\_j}, P_{\Theta_{T\_j}}\right\}, j = 1 \dots N_{\Theta_T}$.
- Target velocity: $V_T \sim \mathrm{N}\left(\mu_{V_T}, {\sigma_{V_T}}^2\right)$; $\overline{\mathrm{V}_T} = \left\{v_{T\_k}, P_{\mathrm{V}_{T\_k}}\right\}, k = 1 \dots N_{\mathrm{V}_T}$.
- Target heading: $\Phi_T \sim \mathrm{N}\left(\mu_{\Phi_T}, {\sigma_{\Phi_T}}^2\right)$; $\overline{\Phi_T} = \left\{\phi_{T\_l}, P_{\Phi_{T\_l}}\right\}, l = 1 \dots N_{\Phi_T}$.

Range/bearing aspects of the resultant target track distribution can be transformed from polar (r, θ) coordinates to Cartesian (x, y) coordinates to yield a probability of target location distribution. The revised target track location then comprises the two random variables X_T and Y_T for the x and y coordinates. This location distribution can be approximated as a discrete probability distribution on a $N_{X_T} \times N_{Y_T}$ Cartesian grid with a specified grid size, e.g. 1 m by 1 m. Each i, j grid cell, $i = 1 \dots N_{X_T}$, $j = 1 \dots N_{\mathrm{Y}_T}$, has x_i, y_j values equal to the midpoint Cartesian coordinates of the cell and probability P_{X_i,Y_j} calculated from the random variables R_T and Θ_T. Two methods were considered for obtaining P_{X_i,Y_j}:

- Approximation of R_T and Θ_T using the discrete random variables $\overline{R_T}$ and $\overline{\Theta_T}$. The x_i, y_j coordinates for each Cartesian grid cell are transformed back to (r, θ) coordinates. The (r, θ) coordinates are then used to obtain probability estimates P_{R_T} and P_{Θ_T} for the grid cell through interpolation of probability values from the discrete distributions $\overline{R_T}$ and $\overline{\Theta_T}$. The probability of target location for the grid cell is then given by $P_{X\_i,Y\_j} = P_{R_T} P_{\Theta_T}$. This method was found to give satisfactory results after renormalisation and reflects a discrete analog to the transformation method for continuous random variables, with interpolation on the discrete probability mass function akin to usage of the continuous probability density function. An alternative method also considered was to computing x_i, y_j and associated probability $P_{R_{T\_i},\Theta_{T\_j}} = P_{R_{T\_i}} P_{\Theta_{T\_j}}$ for each combination of r_{T_i} and θ_{T_j} points in the discrete distributions $\overline{R_T}$ and $\overline{\Theta_T}$. Aggregation of probabilities for all points

[2] For the normally distributed random variable $R \sim \mathrm{N}(\mu, \sigma^2)$, μ represents its mean and σ its standard deviation. This random variable assigns probabilities using the normal cumulative distribution function to ranges of possible values that the variable may take on.

[3] The n-sigma discrete approximation $\bar{R} = \{r_i, P_i\}, i = 1 \dots N$, to $R \sim \mathrm{N}(\mu, \sigma^2)$ is done over the interval $(\mu - n\sigma, \mu + n\sigma)$ using N equally-spaced points across n standard deviations of the normal distribution. The point r_i represents the interval $(\mu - n\sigma + (i-1)\Delta r, \mu - n\sigma + i\Delta r)$ for the normally distributed random variable and is given a value at the midpoint of this interval, where $\Delta r = 2n\sigma/N$. The associated probability P_i is obtained by integrating the probability density function for R across this interval.

mapped into each Cartesian grid cell permits the grid cell`s probability to be determined. This results in a transformed probability distribution over the Cartesian grid, but with possible gaps or irregularities due to the sampling size N_{R_T}, N_{Θ_T} with rounding and summing for mapping into the grid. Increasing the sampling size reduces the gaps and irregularities at the expense of increased computational cost to construct the transformed distribution. The gaps and irregularities can also be numerically smoothed through interpolation for the grid and the resultant distribution renormalized.

- A direct transformation of the joint probability density function for R_T and Θ_T to that for X_T and Y_T using techniques from [2]. This requires obtaining the inverse transformation from (r, θ) to (x, y) and its Jacobian. The resultant joint probability density function for X_T and Y_T can then be integrated across each of the grid cells to obtain the discrete probability of location. This is a more involved method to implement but yields improved results with no errors that otherwise arise when using discrete distribution approximations.

Target Manoeuvre

The target track probability distribution, which reflects known target information at the time of firing, can be projected forward in time in accordance with adopted manoeuvre assumptions to yield a probability distribution for target location at the time of warhead detonation. The time used for this projection is equivalent to the flight time t calculated for the projectile to intercept an aim point based on the target following its default track (mean range, bearing, velocity and heading) with no manoeuvres.

A simple target manoeuvre model was adopted for further analysis and is shown in Figure 1.The target is assumed to be travelling straight at the commencement of firing. The target then initiates a constant speed left or right turn with a prescribed turning radius at some time up to the detonation of the first round[4]. The time at which the turn is initiated is spread evenly across the time interval and the turn is then maintained until the last round has detonated.

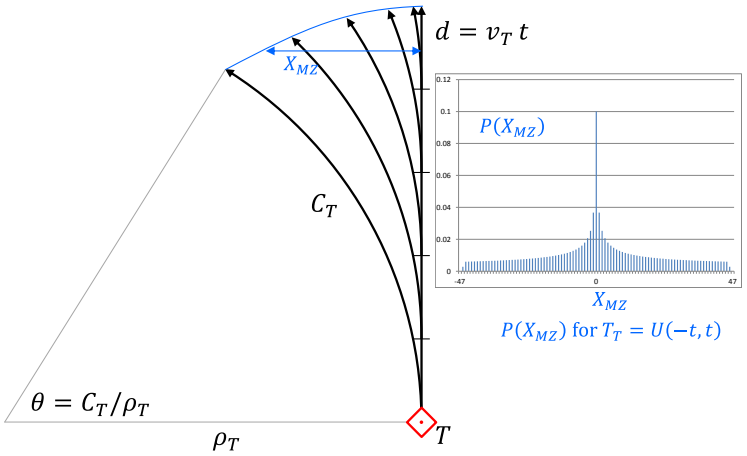

Figure 1. *Target manoeuvre model*

In Figure 1 the target is initially located at point T. The manoeuvre involves straight travel for t_S seconds followed by a constant speed turn with turn radius ρ_T for t_T seconds. The total time of the manoeuvre, which equals the fly-out time of the projectile, is $t = t_S + t_T$. The turning time is

[4] This loosely equates to one leg of a weaving path adopted by a target in which straight segments are randomly mixed with turning segments.

assumed to be an uniformly distributed random variable $T_T \sim \mathrm{U}(-t, t)$, negative values indicating a left turn, positive values indicating a right turn and the absolute value giving the turning time t_T. Figure 1 insert shows the resultant probability distribution for the lateral offset distance X_{MZ} from the default straight manoeuvre that arises for $t_T = |T_T|$. A characteristic feature of this is the spike in probability for X_{MZ} at 0, which arises due to decreasing lateral offsets as t_T approaches 0. Also shown are the left turning manoeuvres corresponding to various values of t_T, ranging from t (curve C_T) to 0.The turning angle θ (in radians) is illustrated for curve C_T.

The target track distribution and target manoeuvre model are used to numerically construct the target movement zone as a discrete joint probability distribution for target location at the time of warhead detonation. For this, initial target location is given from above as a discrete probability distribution on the $N_{x_T} \times N_{y_T}$ grid. Target velocity and initial heading are approximated using their discrete random variables $\overline{V_T}$ and $\overline{\Phi_T}$. The target manoeuvre turning time T_T is also approximated using the discrete random variable $\overline{T_T} = \{t_{T\_m}, P_{T\_m}\}, m = -N_T, -N_T + 1, \ldots, N_T$, where $t_{T\_m} = m\Delta t$ and $\Delta t = t/N_T$. This allows for left/right turns and gives a total of $2N_T + 1$ manoeuvres.

The discrete probability distribution for the movement zone is obtained by looping across each grid point comprising the target track distribution and each sample point in the discrete distributions for target velocity and heading. The target manoeuvre model is then applied for each turning time / probability point from its discrete distribution. The probability for the resultant manoeuvre point is $P_{R_{T\_i}} P_{\Theta_{T\_j}} P_{V_{T\_k}} P_{\Phi_{T\_l}} P_{T\_m}$.This approach leads to $N_{x_T} \times N_{y_T} \times N_{V_T} \times N_{\Phi_T} \times (2N_T + 1)$ manoeuvre calculations and probability aggregations. The result is a discrete probability distribution for the target movement zone giving a probability of target location $P(L_{i_T, j_T})$ for each i_T, j_T cell in an $N_{x_M} \times N_{y_M}$ grid.

Figure 2. shows four target movement zones calculated using this approach. The blue ellipse represents the uncertainty in the target's actual current position, relative to its measured position. Target tracks were computed using $\mu_{R_T} = 4000$ m, $\mu_{\Theta_T} = 0^0$, $\mu_{V_T} = 20$ m/s, $\mu_{\Phi_T} = 180^0$, $\sigma_{R_T} = 10$ m, $\sigma_{\Theta_T} = 1$ mrad, $\sigma_{V_T} = 1$ m/s, $\sigma_{\Phi_T} = 2^0, N_{R_T} = N_{\Theta_T} = 41, N_{V_T} = 3, N_{\Phi_T} = 5$. The resulting grid used to capture the initial target location was of size $N_{x_T} = 100, N_{y_T} = 40$.

A movement zone consisting of a single straight manoeuvre on a grid of size $N_{x_M} = 119, N_{y_M} = 55$ is shown in Figure 2.a. This zone was calculated using 60,000 initial condition/manoeuvre combinations in approximately 2 s on a 2.8 GHz Intel Core 2 Duo CPU. The movement zone shows a translation of the initial track location distribution with slight spreading in the x and y directions due to the velocity and bearing deviations.

Figure 2.b shows the movement zone resulting when nine manoeuvres (four left, four right and one straight) are considered, $\rho_T = 100$ m. Local minima in probability due to each of the individual manoeuvres are clearly present. The figure also shows a concentration of five manoeuvres in the vicinity of the straight manoeuvre, this corresponding to the spike in probability for $X_{MZ} = 0$ shown in Figure 1. Total computing time for this case was 6 s.

A better approximation to the movement zone can be obtained by increasing the number of manoeuvres used in its derivation. Figure 2.c shows the resulting movement zone when 17 manoeuvres are used. The probability distribution has been smoothed with no visible indication of local minima due to individual manoeuvres. Total computing time is 10 s. The effects of a reduced turn radius are shown in Figure 2.d, where $\rho_T = 50$ m. In this case the number of manoeuvres used to construct the movement zone has been increased to 29, given the larger manoeuvre space. Total computing time has increased to 17 s.

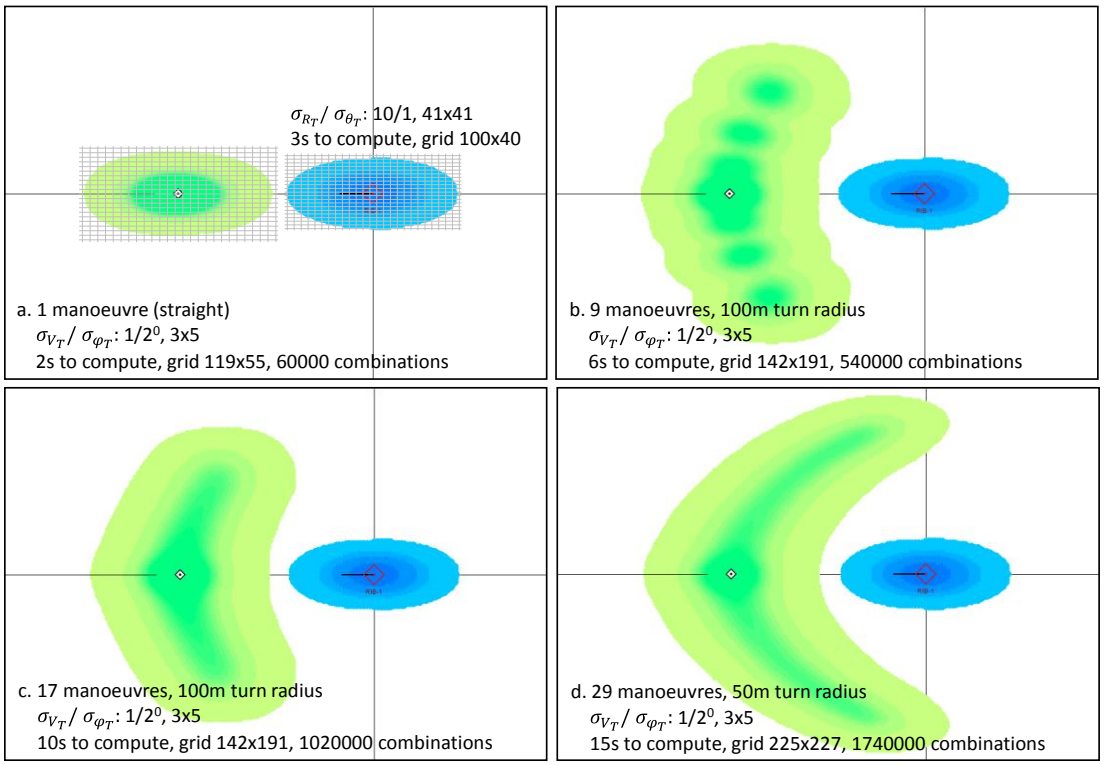

Figure 2. *Target movement zones: a. $N_T = 0$; b. $N_T = 4$, $\rho_T = 100\ m$; c. $N_T = 8$, $\rho_T = 100\ m$; d. $N_T = 14$, $\rho_T = 50\ m$*

Warhead Lethality

Warhead lethality is considered through three aspects: projectile trajectory to determine detonation points; warhead detonation to yield a warhead lethal zone; and aggregation of the warhead lethal zone across possible detonation points to give an aim point lethal zone.

Projectile Trajectory

A spin stabilised projectile with initial muzzle velocity v_0, quadrant elevation angle ε_0, and azimuth angle ψ_0 is fired from a gun at an aim point computed on the basis of available target track information. Projectile file-out is subject to atmospheric conditions, namely air temperature, pressure and density, and aerodynamic forces acting on the moving projectile. Wind may be present but is neglected for this analysis.

Various models are available to represent the external ballistics of a spin stabilised projectile, e.g. the Point Mass (PM) trajectory model [3, 4] and the Modified Point Mass (MPM) model [4]. Both of these models have been implemented and validated using available data. For the results presented below, the PM model from [3] with a constant and illustrative drag coefficient has been used. This model provides two-dimensional trajectories as drift due to Magnus effect and overturning moment are neglected. Such drift acts a bias for the trajectory and would be corrected by an adjustment in azimuth angle during aiming by the FCS.

The FCS estimates for target range, bearing, velocity and heading are used by the ship`s gun control system to compute a ballistics solution for engaging the target. This solution will comprise elevation and azimuth aiming angles and flight time before detonation for the time

fusing mode of the warhead. On firing, the actual aiming angles and muzzle velocity will have small dispersions from the values used in the ballistics calculation. These factors may therefore be viewed as random variables and their dispersions are assumed to be normally distributed. The following continuous random variables with discrete approximations are taken:

- Muzzle velocity: $V_0 \sim \mathrm{N}\left(\mu_{V_0}, {\sigma_{V_0}}^2\right)$; $\overline{V_0} = \left\{v_{0\_i}, P_{V_{0\_i}}\right\}, i = 1 \ldots N_{V_0}$.
- Elevation angle: $\mathrm{E}_0 \sim \mathrm{N}\left(\mu_{\mathrm{E}_0}, {\sigma_{\mathrm{E}_0}}^2\right)$; $\overline{\mathrm{E}_0} = \left\{\varepsilon_{0\_j}, P_{\mathrm{E}_{0\_j}}\right\}, j = 1 \ldots N_{\mathrm{E}_0}$.
- Azimuth angle: $\Psi_0 \sim \mathrm{N}\left(\mu_{\Psi_0}, {\sigma_{\Psi_0}}^2\right)$; $\overline{\Psi_0} = \left\{\psi_{0\_k}, P_{\Psi\_k}\right\}, k = 1 \ldots N_{\Psi_0}$.

The projectile trajectory model takes these variables as inputs and derives output random variables for the detonation point (x, y, z in Cartesian coordinates) and velocity vector (magnitude, elevation and heading angles) of the projectile at detonation, these variables being denoted $\{X_D, Y_D, Z_D, V_D, \mathrm{E}_D, \Psi_D\}$. The trajectory model therefore acts as a function to transform the random variables $\{V_0, \mathrm{E}_0, \Psi_0\}$ to $\{X_D, Y_D, Z_D, V_D, \mathrm{E}_D, \Psi_D\}$. Again, statistical techniques as given in [2] can be used to derive the probability distributions for the transformed variables.

For the analysis below, the discrete distribution approximations for the input variables were used to construct a discrete joint probability distribution for detonation points based on a given aim point. A ballistics solution is obtained for every combination of points from these distributions, for which the associated probability is $P_{i,j,k} = P_{V_{0\_i}} P_{\mathrm{E}_{0\_j}} P_{\Psi\_k}$. This probability is denoted $P(D)$ for the detonation point D. A total of $N_{V_0} \times N_{\mathrm{E}_0} \times N_{\Psi_0}$ ballistics calculations are carried out to construct the detonation point distribution. The outputs from each ballistics calculation, namely $\{\mathrm{x}_D, \mathrm{y}_D, \mathrm{z}_D, \mathrm{v}_D, \varepsilon_D, \psi_D\}$ and associated probability $P(D)$, are used as inputs to the warhead detonation model for calculating the aim point lethal zone.

Warhead Detonation

A simple and idealised fragmentation model has been developed to permit determination of warhead lethal zones. The warhead is assumed to contain N_W spherical fragments of equal size and mass. For a static detonation of the warhead at 0^0 incidence to the horizontal plane, the fragments are ejected evenly in the volume of space defined by the 360^0 rotation of a δ_W wide fan about the warhead's axis of symmetry. The fan is centred on the vertical plane through the midpoint of the warhead and perpendicular to the axis of symmetry, as shown in Figure 3.a. Each fragment is ejected with an initial velocity vector $\tilde{v}_{F_S}$, this being a function of the ejection angles relative to a Cartesian coordinate system centred on the detonation point. Fragment initial velocity, given by $\left|\tilde{v}_{F_S}\right|$, is assumed to be constant for all fragments.

For a dynamic detonation of the warhead the following initial conditions are provided from the warhead trajectory at the time of detonation: projectile velocity vector $\tilde{v}_P$, projectile inclination angle ε_P and detonation height z_P. For each fragment the ejection velocity will be a vector addition of its static velocity vector $\tilde{v}_{F_S}$, which takes into account the ejection angles, and the projectile velocity vector, i.e. $\tilde{v}_F = \tilde{v}_{F_S} + \tilde{v}_P$. The volume of revolution containing the fragment spray has now been pushed forward and tilted downward, as shown in Figure 3.b.

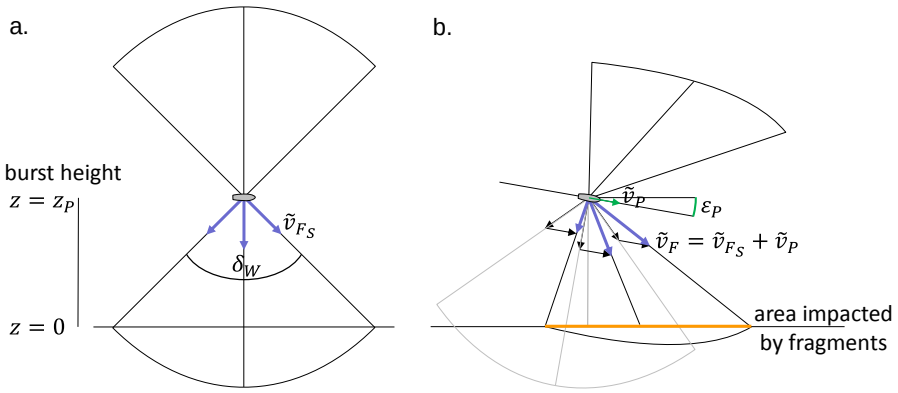

Figure 3. *Warhead fragmentation: a. Static warhead: 0^0 incidence; b. Moving warhead: ε_P incidence and $\tilde{v}_P$ velocity*

Fragment motion through the air is subject to a drag force, this being calculated from the fragment diameter, drag coefficient for a sphere (taken from [5]) and fragment velocity squared. The gravitational force is neglected as it only makes a small contribution for the velocities and distances involved. The solution for this problem shows the velocity to have an approximate linear relationship with distance r traveled. The slope for this relationship is denoted

$$\kappa = \frac{d\tilde{v}_F}{dr} \ . \tag{1}$$

The constant κ was found to be 13.7 s^{-1} for steel pellets 4 mm in diameter, and 8.6 s^{-1} for tungsten pellets with a similar mass.

Those fragments ejected towards the surface will travel a distance r_{xyz} before impacting the surface with impact velocity denoted by v_I. The energy for these fragments is given by

$$E = \frac{1}{2} m_F {v_I}^2 \ , \tag{2}$$

where m_F is the fragment mass. The fragment is considered to cause damage when this energy is greater than a minimum threshold energy E_T, which was taken from [6] to be 80 J. The minimal impact velocity is then given by

$$v_{I\_min} = \sqrt{\frac{2E_T}{m_F}} \ . \tag{3}$$

With equation (1), the minimum ejection velocity for a fragment to carry sufficient energy to equal the threshold energy at impact is then

$$v_{F\_min} = v_{I\_min} + \kappa \, r_{xyz} \ . \tag{4}$$

This defines a lower bound on ejection fragment velocity for determining efficient fragments, i.e. those that have $E \geq E_T$ on impact with a target placed at the sea surface. Target kill assessment is based on determining the probability of these fragments impacting the target.

The intersection of the fragment spray volume with the sea surface defines an area on the surface within which fragment hits occur. Considering each 1 m^2 element in a Cartesian grid for this area, the distance r_{xyz} to the detonation point and the corresponding ejection velocity are calculated. If $|\tilde{v}_F| \geq v_{F\_min}$ for the fragments directed towards the area element, the fragment density (number per m^2) directed towards the element is calculated using

$$d_F = \frac{2N_W}{\pi\delta_W}\left(\tan^{-1}\frac{1}{2r_{xyz}}\right)^2 . \quad (5)$$

This density times the vulnerable area A_T for the target then gives the expected number of impacting efficient fragments striking the target. Following [7], the probability of killing the target, given it is in location $L_{i,j}$ and the detonation occurred at point D, is given by:

$$P\left(K|L_{i,j},D\right) = 1 - e^{-d_F A_T} . \quad (6)$$

This assumes the number of efficient fragments hitting the target forms a Poisson distribution and a kill is achieved if at least one fragment hit occurs. Here, the indices i,j are used to respectively loop across all x,y grid cells on the surface and D indicates an x,y,z detonation point with projectile velocity $\tilde{v}_P$ and inclination angle ε_P.

The warhead lethal zone for a given detonation point D can be numerically constructed through the following steps:

- Loop across each grid cell on the surface. For each i,j grid cell:
  - Determine the r_{xyz} distance to the detonation point.
  - Determine the fragment ejection angles and corresponding $\tilde{v}_F$ from the detonation point to the grid cell.
  - If $|\tilde{v}_F| \geq v_{F\_min}$, determine the fragment density d_F at the grid cell and the corresponding $P\left(K|L_{i,j},D\right)$. Aggregate this probability into the probability distribution for the warhead lethal zone.

Figure 4 shows four warhead lethal zones produced for detonation heights of 1 m, 6 m, 12 m and 18 m. The fragmentation patterns show a typical “butterfly wing” shape that moves forwards with the wings combining as the detonation height increases. The results also show a reduction in maximum probability of kill for increased detonation heights, as the increased distance affects the impact velocity and number of impacting fragments. These patterns are qualitatively similar to those given in [8], obtained through alternative modeling methods, and [6, 9], showing results using data collected from Arena trials.

Aim Point Lethal Zone

The previous sections provide the following key inputs for determining an aim point lethal zone:

- Detonation point probability distribution: $P\left(D_{i_D}\right)$, where $i_D = 1 \ldots N_D$ indicates the detonation point. Each detonation point has an xyz coordinate, projectile velocity $\tilde{v}_P$ and inclination angle ε_P.
- Warhead lethal zone probability distribution: $P\left(K|L_{i,j},D_{i_D}\right)$, where $L_{i,j}$ indicates the i,j grid cell on the surface.

The aim point lethal zone is constructed by calculating the warhead lethal zone for each detonation point and aggregating the resulting probability distributions together. The following relationship holds from the law of total probability:

$$P(K|L_{i,j}) = \sum_{i_D} P(K|L_{i,j} \cap D_{i_D}) = \sum_{i_D} P(K|L_{i,j}, D_{i_D}) P(D_{i_D}) \ , \tag{7}$$

noting that $L_{i,j}$ and D_{i_D} are independent[5]. The aim point lethal zone is obtained by summing across all detonation points the product of kill probability from the warhead lethal zone (for a given detonation point) with the detonation point probability.

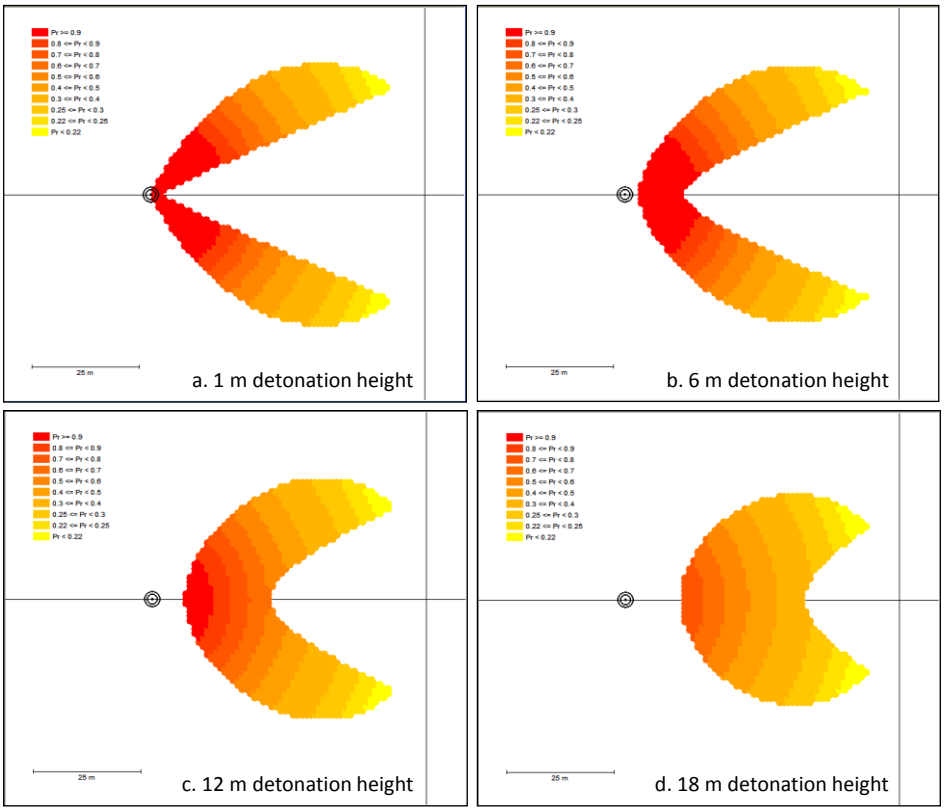

Figure 4. *Height dependency of warhead fragmentation patterns*

Figure 5 presents four aim point lethal zones obtained from detonation point probability distributions constructed using discrete distributions for muzzle velocity and elevation and azimuth angles. In Figure 5.a, a coarse sampling of only three points for the three input discrete distributions is used. The discretization effects are clearly evident, with three main groupings for the three samples of muzzle velocity, each of these having three elevation and three azimuth samples. A total of 3x3x3=27 unique detonation points were used for this aim point lethal zone.

In Figures 5.b and 5.c, the number of samples of the input discrete distributions was respectively increased to 9x7x7=441 samples covering 2-sigma of the normal distributions, and

[5] This assumption can be relaxed by incorporating the aim point, which is dependent on initial target track, and linking target location to initial target track.

25x11x11=3025 samples covering 3-sigma. The aim point lethal zones show a broadening and smoothing with the increase in samples. Figure 5.d shows the resulting aim point lethal zone for 25x11x11 samples when the dispersion errors are halved, the zone being much more compact. Computational time for this case has decreased from that for 7.c as the numerical grid covering the lethal zone is reduced resulting in fewer grid points being used in the calculations.

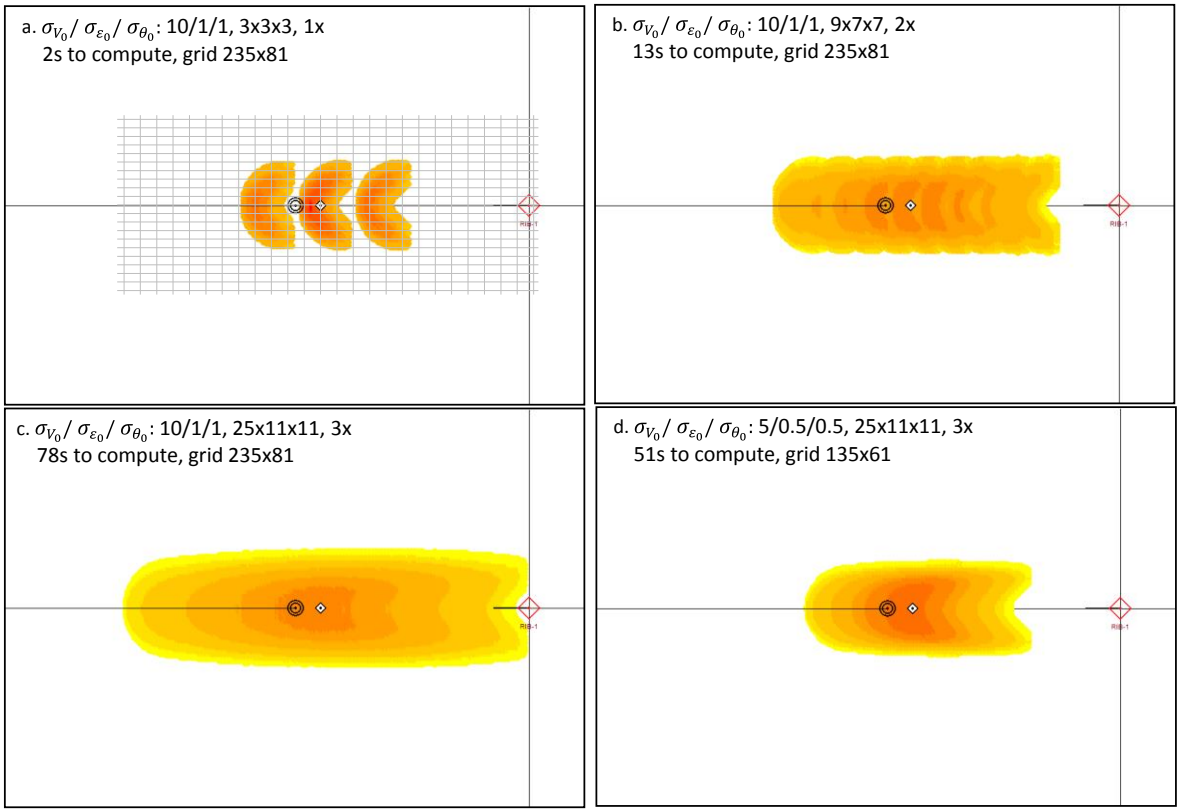

Figure 5. *Aim point lethal zones: a. coarse 3x3x3 solution; b. moderate 9x7x7 solution; c. refined 25x11x11 solution; d. refined solution for reduced dispersions*

Kill Assessment

The selection of an aim point so that its lethal zone overlaps the movement zone of a target will result in a probability that the target will be killed. Single round kill assessment is performed by integrating the product of these two probability distributions over the overlap area. The target movement zone is then updated to reflect target survivability after the first round and used for kill assessment of follow-on rounds. In this manner salvo kill assessment can be performed.

Single Round Kill Assessment

An aim point is specified with respect to a target movement zone computed for a target track. The lethal zone for this aim point may then be integrated across the movement zone to yield a probability of kill for the aim point. The following definitions are used for the input distributions:

- The target movement zone is defined by a grid of x, y cells on the surface. The probability the target is located in the i_T, j_T cell, $i_T = 1 \ldots N_T$, $j_T = 1 \ldots M_T$, at the time of warhead detonation is given by $P\left(L_{i_T, j_T}\right)$.

- The aim point lethal zone is defined by a grid of x, y cells on the surface for an aim point placed at the grid cell corresponding to i_A, j_A. The probability that the target is killed given it is located in grid cell i_T, j_T and the aim point is located in cell i_A, j_A is given by $P\left(K|L_{i_T,j_T}, A_{i_A,j_A}\right)$.

These definitions assume the two distributions overlap. The following summation[6] is then performed to yield the probability of kill for a given aim point A_{i_A,j_A}:

$$P\left(K|A_{i_A,j_A}\right) = \sum_{i_T}\sum_{j_T} P\left(L_{i_T,j_T}\right) P\left(K|L_{i_T,j_T}, A_{i_A,j_A}\right) \ . \tag{8}$$

This equation can be used to determine the optimal aim point that maximises the probability of kill. Two steps are taken for this using a Cartesian coordinate system aligned so that the projective trajectory is in the positive x direction. The first step involves finding for each j_A (giving the aim point y coordinate) the value of i_A (for the x coordinate) that maximises the probability of kill, i.e.

$$P(K)_{max\,j_A} = \max_{i_A} P\left(K|A_{i_A,j_A}\right) \ . \tag{9}$$

The value of i_A that maximises this equation is denoted by i_{A_max} and is a function of j_A. The resulting set of $i_{A\_max}(j_A), j_A$ points defines a max $P(K)$ curve across the target movement zone. The value of j_A that maximises $P(K)$ across this curve, denoted by j_{A_max}, with its corresponding value of $i_{A\_max}\left(j_{A\_max}\right)$ from the curve then gives the location of the optimal aim point. The $P(K)$ for this point is given by:

$$P(K)_{max} = \max_{j_A} P(K)_{max\,j_A} \ . \tag{10}$$

Equations (8, 9, 10) form the basis for computing single round probability of kill. Aspects of the computer implementation include:

- The target movement zone was implemented as a data object consisting of a grid of cells with locations relative to the projected target location L_{i_0,j_0} obtained when no errors and manoeuvres are present. $P\left(L_{i,j}\right)$ is calculated and stored in each grip point in the movement zone.
- The aim point lethal zone was implemented as a data object consisting of a grid of cells with locations relative to an aim point A_{i_0,j_0}, this being defined using the reference point for the target movement zone. $P\left(K|L_{i,j}, A_{i_0,j_0}\right)$ is calculated and stored for each grid point in the lethal zone.
- Methods were implemented permitting translation of either the target movement zone or the aim point lethal zone by respectively translating just L_{i_0,j_0} or A_{i_0,j_0}. This approach assumes small translations will have only a small effect on the corresponding probability distributions and permits kill assessments to be performed efficiently without having to recalculate the translated probability distributions.

[6] This summation follows from application of the law of total probability for the input discrete distributions and is the discrete equivalent to integration for continuous probability distributions.

- The reference points L_{i_0,j_0} and A_{i_0,j_0} are used to align the target movement zone and aim point lethal zone to perform the calculations in equations (8, 9, 10).

This method permits the aim point $A_{i_{A\_max},j_{A\_max}}$ to be determined that maximises the probability of killing the target given its movement zone at the time of detonation. Using this aim point results in the probability $P\left(K|L_{i_T,j_T},A_{i_{A\_max},j_{A\_max}}\right)$ that the target located in cell i_T,j_T is killed. The probability the target survives in this location is then given by:

$$P\left(S|L_{i_T,j_T},A_{i_A,j_A}\right)=1-P\left(K|L_{i_T,j_T},A_{i_A,j_A}\right)\ . \tag{11}$$

Multi-Round Kill Assessment

Equation (11) represents the probability the target continues to be alive in location i_T,j_T after detonation of the first round. For a static target, this equation could then be used directly to provide the probability of target location for kill assessment of a follow-on second round, i.e. $P^2\left(L_{i_T,j_T}\right)=P^1\left(S|L_{i_T,j_T},A_{i_A,j_A}\right)$, where the superscript 1 indicates the result after the first round and the superscript 2 indicates the input for the second round. Equations (8, 9, 10) can then be used to determine the optimal placement of the aim point for round 2, given the round 1 placement. This process can then be applied for further rounds in a salvo.

A similar approach can also be used for moving targets, but with some further complications. The requirement is to update target survivability and evolve the target movement zone to the time point for the detonation of the second round. For the first round, $P^1\left(L_{i_T,j_T}\right)$ comprises contributions from multiple manoeuvres that move the target to the location i_T,j_T, each of these with a specific probability arising from the methods presented above for generating target movement zones. The probability $P^1\left(S|L_{i_T,j_T},A_{i_A,j_A}\right)$ must therefore be applied across these input manoeuvres and used to generate the target movement zone $P^2\left(L_{i_T,j_T}\right)$ for the next time point. This process permits the effects of round 1 warhead detonation to be applied to the contributing manoeuvres, noting further movement using these manoeuvres may result in the target having different locations for the next time point.

A further complication for multi-round kill assessment is placement of the aim points so as to obtain a global optimal solution. One method is to do a brute force search, varying each aim point sequentially through all possible locations (bounded by the input movement locations). This, however, is computationally intensive, increasing exponentially with the number of rounds.

A second method is to place each round using equations (8, 9, 10) in the order of firing, given placement of the previous rounds. After each placement, equation (11) is used to update the probability distribution across the set of manoeuvres, these then being used to determine the probability of target location for the next round/time step. This method leads to “good”, but not globally optimal, solutions. Further improvements can be found by performing a local search about these aim points along the max $P(K)$ curves for each round, noting that movement of an aim point for one round in the salvo requires the movement zones with probabilities of location for subsequent rounds to be re-computed. Restricting aim point placement to locations on the max $P(K)$ curves reduces the amount of movement zone recalculation required and leads to finding better solutions without excessively increasing total computational time.

Illustrative Firing Pattern Results

Figure 6 presents kill assessment results for a four round salvo using aim point lethal zone 4 (from Figure 5.d) and movement zone 3 (Figure 2.c). For these results the range to target was

4000 m and the detonation height was 11 m. In Figure 6.a, the aim points, with corresponding PKs displayed underneath the aim point symbols, are located a short lead distance before the reference points for the corresponding the target movement zones. The lethal zone for the fourth round and its corresponding movement zone are shown in the figure. The total salvo PK = 0.24997, which equals the sum of the individual round PKs, is displayed under the target symbol. Also shown spanning the movement zone are the max $P(K)$ curves for the four rounds, upon which each of the round aim points are located.

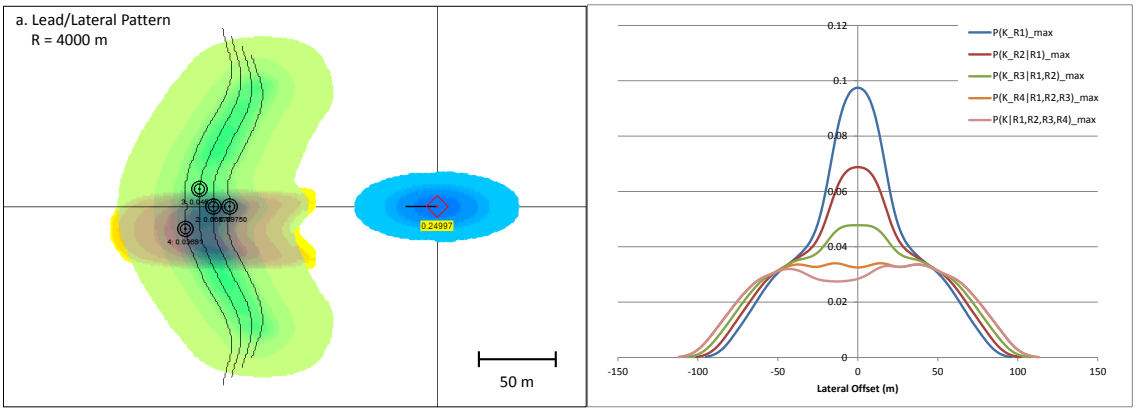

Figure 6. *Four round results: a. round laydown; b. max $P(K)$ curves*

Figures 6.b shows a plot of the max $P(K)$ curves for the four rounds, these being functions of $y(j_A)$ calculated using equation (9). It should be noted that the curves for rounds 2 to 4 are dependent on placement of the aim points for the previous rounds in the salvo. Equation (10) involves choosing j_A so that $P(K)$ for each of the rounds is maximised from these curves, which was done for rounds 1, 2 and 4. The placement of the aim point for round 3 was done through a local search to obtain a better solution for the salvo. The resulting solution, with lateral offsets of the aim points from the line of sight to the target, is:

- Round 1: $P^1(K) = P^1(K)_{max} = 0.09750$ at $y(j_A) = 0$ m.
- Round 2: $P^2(K) = P^2(K)_{max} = 0.06878$ at $y(j_A) = 0$ m.
- Round 3: $P^3(K) = 0.04706$ at $y(j_A) = 9.6$ m.
- Round 4: $P^4(K) = P^4(K)_{max} = 0.03660$ at $y(j_A) = -14$ m.
- Salvo: $P^{S,4}(K) = \sum_{i_R} P^{i_R}(K) = 0.24994$.

Equations (8, 9, 10) can be used to determine the optimal offset of the detonation point for a single round relative to the target movement zone reference point L_{i_0,j_0}. Figure 7 shows results obtained for a target placed at 2000 m with the detonation point height varied from 0 m to 20 m in steps of 1 m. In Figure 7.a, $P(K)$ is maximised for a detonation height of 13 m. For this height, Figure 7.b shows the optimal x, y offset of the detonation point is 17 m before the target reference point (lead offset) and on the line of sight to the target (0 m lateral offset). The detonation point height obtained from this approach is incorporated into the aim point definition as it is fairly constant. The lead and lateral offsets are used to define the aim point relative to the target movement zone reference location, these varying for each round when considering multiple rounds in a salvo.

Also shown in Figure 7.a is the $P(K)$ dependence on detonation height for a six round salvo with aim points placed in an optimising pattern against a target located at 3500 m range. For this situation an aim point height of 10 m was found to give the maximum salvo probability of kill.

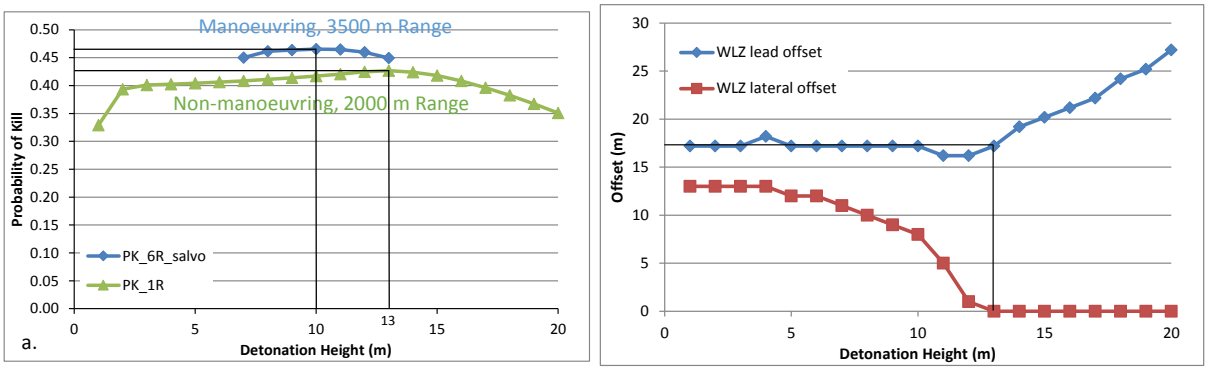

Figure 7. *Optimal aim point: a. height offset; b. lead and lateral offsets*

Figure 8 shows firing patterns with salvo kill probabilities obtained for target ranges from 2000 m to 5000 m in steps of 500 m. Figure 8.d shows a lead only pattern, i.e. no lateral offsets considered, with $P^{S,6}(K) = 0.40855$ for target range 3500 m. Inclusion of lateral offsets permits the pattern shown in Figure 8.e to be obtained, its $P^{S,6}(K) = 0.46470$, an increase of 14%. The remaining patterns in Figure 8 include both lead and lateral offsets in determination of an optimal pattern for each range.

The target track distributions in Figure 8 show a broadening in width as range is increased. This is due to the range dependence of the angular dispersion error when transformed into Cartesian coordinates. The target movement zones show increased translations ahead of the target track distributions, in direction of the target heading, for increasing range. The zones also show an increased lateral spreading with wrapping around the target track distribution for increasing range. Both of these effects are due to the increased time for target travel and turning movement during the longer projectile fly-out times. The zones also show a small increase in thickness, in direction of the target heading, for increasing range, this being due to spreading arising from the target track velocity dispersion.

The results of Figure 8 show the aim point lethal zones to elongate in the direction of the firing line and become narrower about this line for increased ranges. The lethality of the zones also decreases, as shown by the lethal zone heat maps in Figure 8. A number of factors contribute to this behavior. An increase in range will lead to a lengthening and broadening of the detonation point distribution as generated by the ballistics trajectory model. The projectile terminal velocity will become lower and the magnitude of the projectile elevation angle at detonation will also increase. These aspects are direct inputs to the projectile fragmentation model. The decrease in projectile velocity at the time of detonation will lead to a warhead reduced lethal zone on the surface within which fragments have sufficient energy to cause damage. The steeper descent angle at detonation will also throw a higher proportion of fragments backwards, also reducing the lethal zone. Aim point lethal zone elongation is therefore due to the lengthening of the detonation point distribution for increased ranges, this mainly arising from muzzle velocity dispersion error. Its reduction in width is due to the reduced warhead lethal zone at increased ranges, this dominating a tendency to increase arising from the broadening in width of the detonation point distribution.

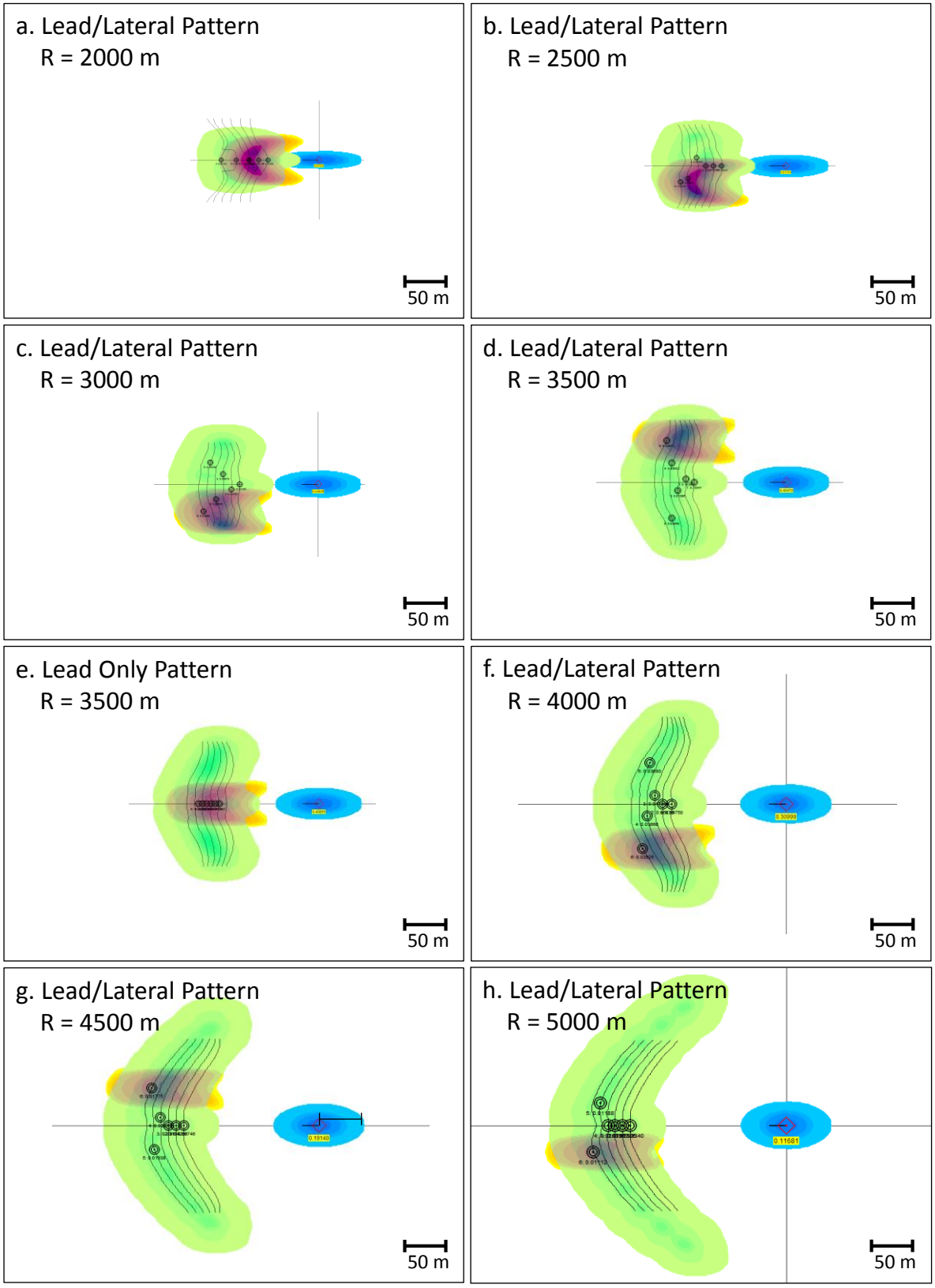

Figure 8. *Six round firing pattern results at ranges 2000 m to 5000 m*

The lead/lateral offset patterns in Figure 8 show the following features:

- No lateral offsets are needed for target range 2000 m as the width of the aim point lethal zone is comparable to that for the target movement zone.
- As range increases, lateral offsets are used for later rounds in the salvo. These increase in magnitude until range 4000 m, after which they decrease.
- Salvo $P^{S,6}(K)$ monotonically decreases from its maximum at range 2000 m, as expected.
- At range 5000 m, only the final two rounds have small lateral offsets. This arises as the salvo $P^{S,6}(K)$ is reduced with all rounds being used in the area of maximum probability for target location near $y(j_A) = 0$ (the spike observed in Figure 1). This reflects the reduced probability of kill at longer ranges resulting in more rounds being needed to achieve a local minimum for PK along the zero-offset axis, after which further rounds would be fired with nonzero lateral offsets. It is expected that additional rounds in a salvo for this range would have increasing lateral offsets as the target location probability becomes flattened across the movement zone.

Figure 9 shows determination of the maximum $P^{S,6}(K)$ for patterns involving only a lead offset, such as that in Figure 8.c, the offsets being found to vary from 27 m for range 2000 m to 18 m for range 5000 m. A comparison of kill probabilities from these simplified patterns to PKs from the patterns involving both lead and lateral offsets in Figure 8 is given in Figure 10. It is seen the difference is small at range 2000 m (< 1%), increases to a maximum of 14% at range 3500 m (corresponding to the maximum magnitudes of lateral offsets for the aim points), and then decreases to 5% at range 5000 m. Figure 11 provides the range dependence of aim point lateral offsets for the lead/lateral offset patterns. Round 1 is not shown in this figure as it always had zero lateral offset for all ranges.

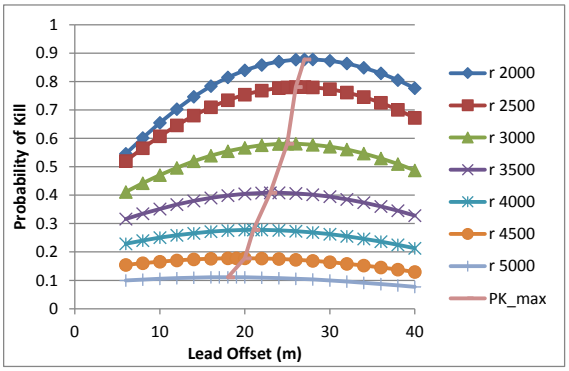

Figure 9. *Determination of optimal lead offset for lead only patterns*

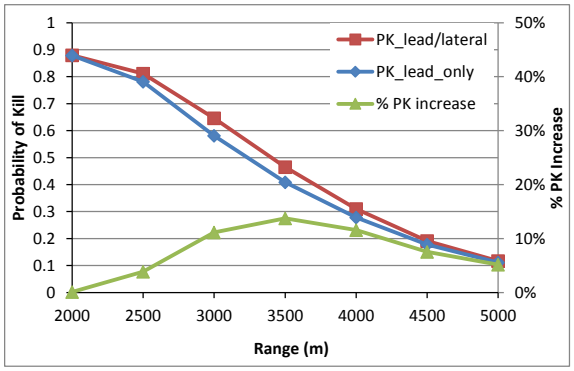

Figure 10. *Comparison of lead only and lead/lateral pattern PKs*

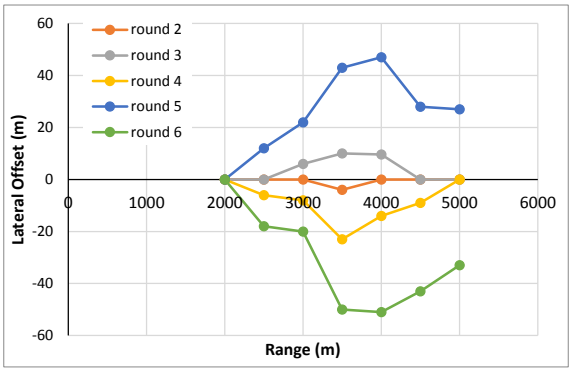

Figure 11. *Range dependence of lateral offsets for lead/lateral patterns*

The results presented above all involved a target heading directly towards the defending ship, i.e. the target and incoming shells were on reciprocal courses. In general, the target heading at the time of firing will vary as it manoeuvres in order to avoid the ship's gunfire. It is therefore of interest to consider other situations where the target heading and manoeuvre assumptions are changed. Two situations are presented in Figure 12 for range 3500 m to illustrate additional features of the generalized engagement problem. In Figure 12.a, the target is given an initial heading of 225^0, i.e. its initial velocity vector has been turned 45^0 to the left from that in Figure 8.d. The same manoeuvre model as for Figure 8.d is used, this being shown in the inset to the figure – Manoeuvre Model 1. The resulting movement zone has been compacted and skewed, i.e. stretched with rotation, due to the major axis of the target track distribution not being aligned with the target velocity vector. The calculated lead/lateral firing pattern achieves a higher salvo PK = 0.49625, when compared to Figure 8.d with PK = 0.46470. This arises as the aim point lethal zones better align with the main ridge of the movement zone probability distribution.

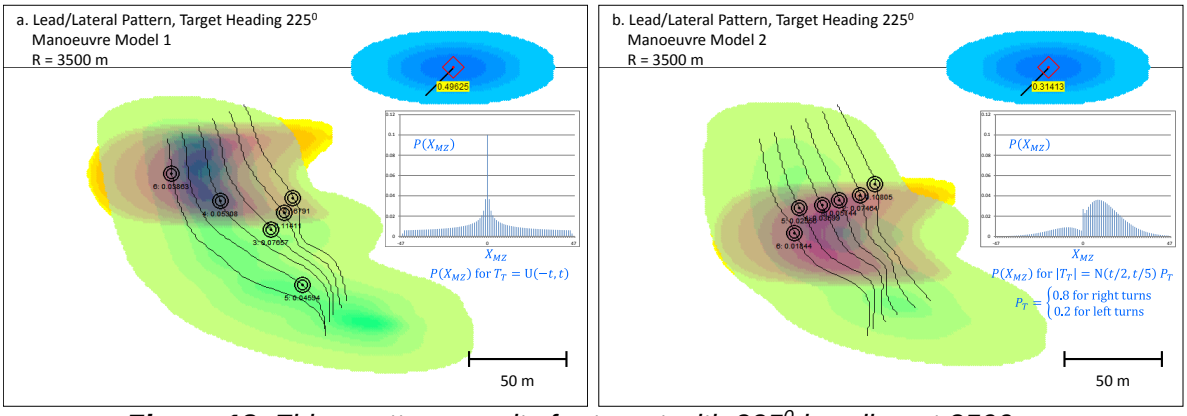

Figure 12. *Firing pattern results for target with 225^0 heading at 3500 m range*

Figure 12.b presents results for the same the engagement situation but with alternative manoeuvre assumptions chosen for illustrative purposes – Manoeuvre Model 2 shown in the inset. This model assumes the target turning time to have a truncated normal distribution over the manoeuvre time t: $T_T \sim \mathrm{N}(t/2, t/5)$ with renormalisation. A 4:1 ratio bias favouring right turns over left has also been introduced, reflecting a higher probability the target will turn towards the ship. The lateral distance offset distribution given in the inset shows the earlier spike at $X_{MZ} = 0$ for Manoeuvre Model 1 is reduced and the probability is now predominantly spread across positive X_{MZ}, this being associated with right turns. The resulting firing pattern is concentrated

on the right turning side of the movement zone and has a reduced salvo PK = 0.31413 due to the target location probability now having a greater spread over the movement zone.

Concluding Remarks

A computational approach has been developed for the determination of firing patterns so as to maximise salvo kill probability for engagement of manoeuvring surface targets. Application of the method using illustrative data has demonstrated some of the characteristics of firing patterns, in particular the range dependence of aim point offsets for individual rounds in a salvo. Actual firing patterns for systems and targets of interest will share these characteristics but demonstrate features dependent upon input dispersion errors and target assumptions.

The main goal of the present work is to support development of firing patterns to be employed by gun systems for combating manoeuvring surface threats. The work presented here has highlighted many of the contributing factors and complexities to the problem, and has demonstrated how statistical-based computational techniques can be applied for its analysis. Additional applications of the work include: evaluation of target manoeuvre assumptions and attack strategies; determination of firing strategies to incorporate optimal open-fire ranges and salvo sizes; and development of heuristic algorithms to capture functional dependence of firing patterns on key input parameters across a range of tactical situations.

Research is ongoing to improve various aspects of the underlying methodology. Direct transformations of continuous random variables are being introduced to reduce discretization errors arising from discrete probability distributions. Track updates received during firing of rounds in a salvo are being used to confine growth of the target movement zone. Numerical and analytical techniques are being investigated for determining optimal aim point offsets. Initial scoping is being performed for extending the methodology to consider manoeuvring air targets.

The methodology is now being applied to support development of gun system firing patterns for the Royal Canadian Navy. Cross model validation is being performed with a Monte Carlo simulation, with both models being used to develop firing patterns. Further validation will be performed through live firing field trials. Model results will also feed into a multi-threat engagement analysis.

References

[1] Naval Gun Firing Patterns Against Manoeuvring Surface Targets, P.J. Young, DRDC-RDDC-2016-L176, 30 May 2016.

[2] Introduction to the Theory of Statistics, A.M. Mood, F.A. Graybill & D.C. Boes, 3rd Ed., McGraw-Hill, New York, USA, 1974.

[3] Projectile Motion with Air Resistance Quadratic in the Speed, G.W. Parker, American Journal of Physics, Vol. 45, No. 7, Jul. 1977.

[4] The Modified Point Mass and Five Degrees of Freedom Trajectory Models, NATO STANAG 4355 JAIS Ed 3, NSA/0454(2009)-JAIS/4355, 17 Apr. 2009.

[5] Bubbles, Drops and Particles, R. Cliff, J.R. Grace and M.E. Weber, Academic Press, New York, U.S.A.,1978.

[6] Lethal Influence Factors of Natural and Preformed Fragmentation Projectiles, B. Zecevic, J. Terzic, F. Razic, & S. Serdarevic-Kadic, Chapter 20 in DAAAM International Scientific Book 2015, pp. 219-234, B. Katalinic (Ed.), DAAAM International, Vienna, Austria, 2015.

[7] Terminal Effectiveness of Anti-Personnel Fragmenting Projectiles, US Army Test and Evaluation Command, Test Operations Procedure, APG, Maryland, U.S.A., Feb., 1982.

[8] Analytic and Probabilistic Techniques for the Determination of Surface Spray Patterns from Air Bursting Munitions, P.A. Chircop, Proceedings of the 24th National Conference of the Australian Society for Operations Research, forthcoming in Springer's Lecture Notes in Management and Industrial Engineering, November 2016.

[9] Comparison of Lethal Zone Characteristics of Several Natural Fragmenting Warheads, B. Zecevic, A. Catovic & J. Terzic, Central European Journal of Energetic Materials, 5(2), pp. 67-81, 2008.